Large-scale evaluation of β-decay rates of r- process nuclei with the inclusion of first- forbidden transitions

Marketin, Tomislav; Huther, Lutz; Martinez-Pinedo, Gabriel

Source / Izvornik: **Physical Review C, 2016, 93**

Journal article, Published version
Rad u časopisu, Objavljena verzija rada (izdavačev PDF)

https://doi.org/10.1103/PhysRevC.93.025805

Permanent link / Trajna poveznica: https://urn.nsk.hr/urn:nbn:hr:217:356275

Large-scale evaluation of β-decay rates of r-process nuclei with the inclusion of first-forbidden transitions

T. Marketin,[1] L. Huther,[2] and G. Martínez-Pinedo[2,3]
[1]*Department of Physics, Faculty of Science, University of Zagreb, 10000 Zagreb, Croatia*
[2]*Institut für Kernphysik (Theoriezentrum), Technische Universität Darmstadt, 64289 Darmstadt, Germany*
[3]*GSI Helmholtzzentrum für Schwerioneneforschung, Planckstraße 1, 64291 Darmstadt, Germany*
(Received 21 July 2015; revised manuscript received 4 January 2016; published 12 February 2016)

Background: r-process nucleosynthesis models rely, by necessity, on nuclear structure models for input. Particularly important are β-decay half-lives of neutron-rich nuclei. At present only a single systematic calculation exists that provides values for all relevant nuclei making it difficult to test the sensitivity of nucleosynthesis models to this input. Additionally, even though there are indications that their contribution may be significant, the impact of first-forbidden transitions on decay rates has not been systematically studied within a consistent model.
Purpose: Our goal is to provide a table of β-decay half-lives and β-delayed neutron emission probabilities, including first-forbidden transitions, calculated within a fully self-consistent microscopic theoretical framework. The results are used in an r-process nucleosynthesis calculation to asses the sensitivity of heavy element nucleosynthesis to weak interaction reaction rates.
Method: We use a fully self-consistent covariant density functional theory (CDFT) framework. The ground state of all nuclei is calculated with the relativistic Hartree-Bogoliubov (RHB) model, and excited states are obtained within the proton-neutron relativistic quasiparticle random phase approximation (pn-RQRPA).
Results: The β-decay half-lives, β-delayed neutron emission probabilities, and the average number of emitted neutrons have been calculated for 5409 nuclei in the neutron-rich region of the nuclear chart. We observe a significant contribution of the first-forbidden transitions to the total decay rate in nuclei far from the valley of stability. The experimental half-lives are in general well reproduced for even-even, odd-A, and odd-odd nuclei, in particular for short-lived nuclei. The resulting data table is included with the article as Supplemental Material.
Conclusions: In certain regions of the nuclear chart, first-forbidden transitions constitute a large fraction of the total decay rate and must be taken into account consistently in modern evaluations of half-lives. Both the β-decay half-lives and β-delayed neutron emission probabilities have a noticeable impact on the results of heavy element nucleosynthesis models.

DOI: 10.1103/PhysRevC.93.025805

I. INTRODUCTION

One of the currently most active fields of nuclear astrophysics deals with the synthesis of elements heavier than iron by the r process. Even though its astrophysical site has not yet been identified, it is commonly accepted that it occurs in explosive environments involving relatively high temperatures (up to 1 GK) and neutron densities ($n_n > 10^{20}$ g cm^{-3}). Apart from the complexities involved in the astrophysical modeling, the r process represents a particularly difficult challenge due to the large amount of nuclear input required. It is a complex, dynamical process involving a delicate interplay between the strong, electromagnetic, and weak interactions, requiring the knowledge of a number of observables in several thousand nuclei across the whole nuclear chart. Among the crucial nuclear properties having a direct impact on the distribution of elemental abundances are the β-decay half-lives of the participating nuclei [1,2]. They determine the speed of matter flow toward higher atomic numbers, setting the timescale for the r process. β-delayed neutron emission occurs during the whole r-process duration but becomes particularly important at late phases when a competition between neutron captures and β decays takes place [3]. Particularly important are the β-decay half-lives of nuclei around magic neutron numbers $N = 50$, 82, and 126. The neutron separation energies show discontinuities around these magic numbers, resulting in rather low neutron capture rates. As a consequence the r-process matter flow moves closer to stability, where nuclei have substantially larger β-decay half-lives. Thus matter accumulates around magic numbers $N = 50$, 82, and 126, producing the observed peaks in the solar system r-process distribution.

At present only a few half-lives of r-process nuclei in the vicinity of the magic numbers $N = 50$ [4–7] and $N = 82$ [8–11] have been measured. Even though the experiments at GSI have provided valuable information for half-lives approaching the third r-process peak [12–16], so far no experimental half-lives for r-process nuclei at the $N = 126$ shell closure are available. Hence, r-process nucleosynthesis calculations rely mainly on theoretical half-lives. The interacting shell model [17] has recently been extended to include first-forbidden transitions and has been applied to the calculation of half-lives for r-process nuclei around $N = 50$, 82, and 126 shell closures [18]. However, due to the increasing computational cost, shell-model calculations are restricted to nuclei near closed shells. For this reason most of the half-lives calculations for r-process nuclei are based on the quasiparticle random phase approximation on top of semiempirical global

models [19–21], the Hartree-Fock-Bogoliubov model [22], or the relativistic Hartree-Bogoliubov model [23–25]. The quasiparticle random phase approximation (QRPA) approach based on a global effective interaction presents a valid alternative to the interacting shell model. It has been successfully employed in numerous applications [26] and can provide a systematic description of β-decay properties of arbitrarily heavy nuclei. The importance of performing calculations based on the self-consistent mean-field models, as opposed to the empirical mean-field potentials has been already emphasized [20]. Currently, however, the only available large-scale calculation of β-decay properties of nuclei used in heavy element nucleosynthesis simulations is based on an QRPA calculation based on a schematic interaction on top of the finite range droplet model (FRDM) [19]. Additionally, in β-decay calculations the impact of first-forbidden transitions on the total decay rate is mostly unexplored. While these transitions and their higher order counterparts have been included in the investigations of electron and muon capture rates and neutrino-nucleus interactions, either their use in β-decay studies has been limited to particular isotopic chains [27] or they have been described using a different theoretical foundation such as the gross theory [19]. Furthermore, due to the existence of a single data table of β-decay half-lives, it is not possible to perform meaningful sensitivity studies on the influence of β-decay rates on r-process nucleosynthesis.

In an effort to avoid effects coming from combining models built on differing theoretical bases, and with the aim of providing a new, high precision data table of β-decay properties, in this study we utilize a fully self-consistent theoretical framework based on the relativistic Hartree-Bogoliubov (RHB) model [28] for the description of the ground state of open- and closed-shell nuclei with the proton-neutron relativistic quasiparticle random phase approximation (pn-RQRPA) where the residual interaction is derived from the same density functional as was used for the ground state calculations. In this way, we ensure the consistency among the various required properties, from the masses and Q_β values to the nuclear response strength functions. The RHB+ pn-RQRPA approach was already successfully employed in the study of Gamow-Teller and higher order resonances [29,30], β-decay half-lives [23,24], and stellar weak-interaction processes [31,32]. This framework also enables the treatment of first-forbidden transitions on an equal footing with the Gamow-Teller transitions, allowing for a meaningful investigation of the contribution of the $J > 0$ modes of nuclear excitation and for studying the regions of interest where this contribution is significant. We use this model to calculate the β-decay half-lives and the β-delayed neutron emission probabilities of 5409 neutron-rich nuclei with $8 \leqslant Z \leqslant 124$, including even-nuclei but also nuclei with an odd number of particles. In Sec. II we present the theoretical formalism of the model, while Sec. III contains all the necessary expressions for the evaluation of matrix elements and nuclear properties, together with the presentation and discussion of obtained results. Finally, in Sec. IV we provide the concluding remarks. The complete data table containing the decay rates, neutron emission probabilities, and released energy is available as Supplemental Material [33].

II. THEORETICAL FORMALISM

A. QRPA calculations

The calculation of β-decay rates requires the calculation of both the nuclear ground state and excited states of the daughter nucleus and the transitions between them, together with the evaluation of the lepton phase space involved in the transition. Because the calculation requires a good description of a wide range of physical quantities, and because the goal is to obtain the decay rates for a very large range of nuclei, we employ a fully microscopic theoretical framework based on the relativistic nuclear energy density functional (RNEDF). The RNEDF based framework employs the self-consistent mean field for nucleons and a minimal set of meson fields; the isoscalar scalar σ meson ($J^\pi = 0^+, T = 0$), the isoscalar vector ω meson ($J^\pi = 1^-, T = 0$), and the isovector vector ρ meson ($J^\pi = 1^-, T = 1$), supplemented with the electromagnetic field. The meson-nucleon interaction is included with a minimal set of the interaction terms, where the vertex functionals include explicit dependence on the nucleon vector density [28]. The nuclear ground state properties are described using the relativistic Hartree-Bogoliubov (RHB) model, which properly describes the pairing effects in open-shell nuclei. For the model parameters that determine the density-dependent couplings and the meson masses, in this work the D3C* parametrization is used [24], as it was previously shown that it provides a good description of β-decay half-lives in medium and heavy nuclei. The pairing correlations in open shell nuclei are described by the finite range Gogny interaction, with the D1S parametrization [34].

The excited states are obtained using the proton-neutron relativistic quasiparticle random phase approximation (pn-RQRPA), formulated in the canonical single-nucleon basis of the RHB model [35] and extended to the description of charge-exchange excitations (pn-RQRPA) [29]. The RHB + RQRPA model is fully self-consistent in both the ph and pp channels. The same interactions are used in the RHB equations that determine the canonical quasiparticle basis, and in the matrix equations of the RQRPA. Transitions between the 0^+ ground state of a spherical parent nucleus and the J^π excited state of the corresponding daughter nucleus are induced by a charge-exchange operator T^{JM}. Assuming spherical symmetry of the nuclear system, the quasiparticle pairs can be coupled to good angular momentum, and the matrix equations of the pn-RQRPA read [36]:

$$\begin{pmatrix} A^J & B^J \\ B^{*J} & A^{*J} \end{pmatrix} \begin{pmatrix} X^{\lambda J} \\ Y^{\lambda J} \end{pmatrix} = E_\lambda \begin{pmatrix} 1 & 0 \\ 0 & -1 \end{pmatrix} \begin{pmatrix} X^{\lambda J} \\ Y^{\lambda J} \end{pmatrix}, \quad (1)$$

where the matrices A and B are defined in the canonical basis [36]. For each energy E_λ, $X^{\lambda J}$ and $Y^{\lambda J}$ in Eq. (1) denote the corresponding forward- and backward-going QRPA amplitudes, respectively. The transition matrix element between the ground state of the parent nucleus and the excited state of daughter nucleus, induced by the operator T^{JM}, reads

$$B^{\pm}_{\lambda J} = \left| \sum_{pn} \langle p||T^J||n\rangle \left(X^{\lambda J}_{pn} u_p v_n + (-1)^J Y^{\lambda J}_{pn} v_p u_n \right) \right|^2. \quad (2)$$

where the X and Y amplitudes are obtained from solving the pn-RQPA equation (1).

In the $T = 1$ channel of the pn-RQRPA we use the pairing part of the Gogny force:

$$V^{pp}(1,2) = \sum_{i=1,2} e^{-r_{12}^2/\mu_i^2} (W_i + B_i P^\sigma - H_i P^\tau - M_i P^\sigma P^\tau), \tag{3}$$

with $r_{12} = |\boldsymbol{r}_1 - \boldsymbol{r}_2|$, P^σ and P^τ are the spin and isospin exchange operators, and the D1S set of parameters μ_i, W_i, B_i, H_i and M_i ($i = 1,2$) are taken from [34]. This force has been carefully adjusted to pairing properties of finite nuclei all over the periodic table. In particular, the basic advantage of the Gogny force is the finite range, which automatically guarantees a proper cutoff in the momentum space. For the $T = 0$ proton-neutron pairing interaction in open shell nuclei we use a form consisting of a short-range repulsive Gaussian combined with a weaker longer-range attractive Gaussian:

$$V_{12} = -V_0 \sum_{j=1}^{2} g_j e^{-\frac{r_{12}^2}{\mu_j^2}} \hat{\Pi}_{S=1,T=0}. \tag{4}$$

where $\hat{\Pi}_{S=1,T=0}$ projects onto states with $S = 1$ and $T = 0$. The ranges $\mu_1 = 1.2$ fm and $\mu_2 = 0.7$ fm of the two Gaussians are taken from the Gogny interaction. The relative strengths $g_1 = 1$ and $g_2 = -2$ are chosen so that the force is repulsive at small distances. The only remaining free parameter is V_0, the overall strength. This interaction, with a constant value of V_0, was used in the nonrelativistic QRPA calculation [22] of β-decay rates for spherical neutron-rich r-process waiting-point nuclei. Two relativistic calculations of β-decay half-lives of neutron-rich nuclei [23,24] have shown that a single value of the overall interaction strength cannot be successfully used in different regions of the nuclear chart. Thus, we take the ansatz proposed in [25],

$$V_0 = V_L + \frac{V_D}{1 + e^{a+b(N-Z)}}, \tag{5}$$

with values $V_L = 160.0$ MeV, $V_D = 15.0$ MeV, $a = 7.2$, and $b = -0.3$ adjusted to obtain the best possible description of available half-life data [37].

The model employed in this study is well suited to describe the properties of the ground state and of the excited states of even-even nuclei. However, as the r process naturally includes odd-A and odd-odd nuclei as well, it becomes necessary to provide at least an approximate description of the decay properties of these nuclei. With this aim, we compute the ground state of odd nuclei by employing the same model as for even-even nuclei, but constraining the expectation value of the particle number operator to an odd number of protons and/or neutrons. In this way an *even* RHB state is obtained, whose energy is different from the *true* odd nucleus ground state energy by the energy of the odd quasiparticle [40,41]. To quantify the validity of this approximation, we show the computed Q_β values for the silver and cadmium ($Z = 45$) isotopic chains in Fig. 1, calculated by approximating the

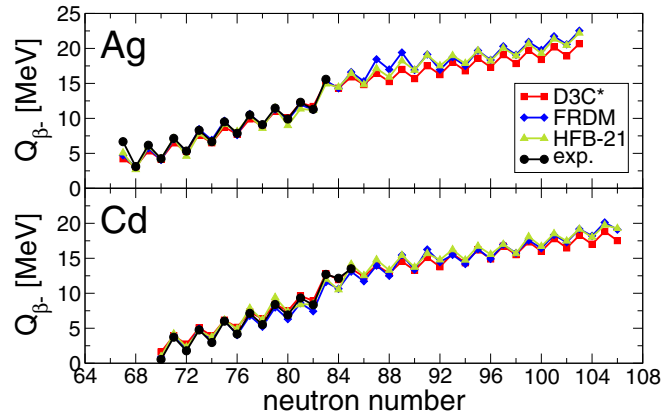

FIG. 1. β-decay Q values for the silver and cadmium isotopic chains. Values calculated in this work, marked with red squares, are compared with the values obtained from the FRDM mass table [38] (blue diamonds), with the HFB-21 model [39] (green triangles), and with existing experimental data [37] (black circles).

binding energy of the daughter nucleus [22]:

$$\begin{aligned} Q &= \Delta M_{nH} + \lambda_n - \lambda_p - E_{2qp} \\ &= M_{ex}(Z,N) - M_{ex}(Z+1,N-1), \end{aligned} \tag{6}$$

where λ_n and λ_p are the neutron and proton Fermi energies in the ground state of the parent nucleus, and E_{2qp} are the lowest quasiparticle energies. $\Delta M_{nH} = 0.782$ MeV is the mass difference between a neutron and the hydrogen atom, and $M_{ex}(Z,N)$ is the mass excess. In silver isotopes (odd Z), the Q_β values are well reproduced for nuclei with an even number of neutrons, and only slightly underestimated for odd-odd nuclei. The predicted values closely follow the jump above the closed neutron shell, and begin to deviate from the FRDM values after the shell closure, while the HFB-21 results are found between the other two models. For the cadmium isotopes the model overestimates the Q_β values in nuclei with an even number of neutrons in lighter isotopes, but above $N = 78$ the results reproduce the experimental values accurately. Again, the model very successfully reproduces the changes around the closed neutron shell. For heavier isotopes there are no available data, but all the models coincide in their predictions of the Q_β values. We can conclude from these results that this approach to estimating the Q values provides a good agreement with the available data and does not hinder our study of weak-interaction processes.

We note that our calculations do not consider the effects of finite temperature in the astrophysical environment. For the temperatures relevant for r-process nucleosynthesis, $kT <$ 100 keV, this approximation is certainly justified for even-even nuclei. The situation may be different for odd and odd-odd nuclei. Takahashi and Yokoi [42] find some sensitivity of the β-decay rates to thermal effects for nuclei very close to stability, with long β-decay rates and small Q values. It is expected that, in moving to neutron-rich nuclei relevant for r-process nucleosynthesis, characterized by large Q values and decay rates, the sensitivity to thermal effects will decrease. This is indeed confirmed by the results of Refs. [43–45].

B. β-decay half-lives

In the present study of β-decay half-lives we include both allowed ($L = 0$) and first-forbidden ($L = 0,1$) transitions. The β-decay rate for a transition between an initial and final nuclear state is equal to [46]

$$\lambda = \frac{\ln 2}{K} \int_0^{p_0} p_e^2 (W_0 - W)^2 F(Z,W) C(W) dp_e, \tag{7}$$

where W is the electron energy in units of $m_e c^2$ with W_0 being the maximum electron energy that is equal to the difference in nuclear masses between initial and final nuclear states, $W_0 = (M_i - M_f)/m_e$, and p_e is the electron momentum in units of $m_e c$. We approximate the maximum electron energy with [22]

$$M_i - M_f \approx \lambda_n - \lambda_p + \Delta M_{nH} - E_{QRPA}. \tag{8}$$

The constant K is measured in superallowed β decay to be $K = 6144 \pm 2$ s [47].

The shape factor $C(W)$ differs for various decays. For allowed decays it is energy independent. In the case of β^- decay of neutron-rich nuclei, the shape factor is simply the Gamow-Teller reduced transition probability, $C(W) = B(GT)$, with

$$B(GT) = g_A^2 \frac{\langle f \| \sum_k \boldsymbol{\sigma}^k \boldsymbol{t}_-^k \| i \rangle^2}{(2J_i + 1)}. \tag{9}$$

The matrix element is reduced with respect to the spin operator $\boldsymbol{\sigma}$ only using the Condon-Shortley phase convection [48]. The sum runs over all nucleons. For the isospin lowering operator we use the convention $t_- |n\rangle = |p\rangle$. Finally, $g_A = -1.2701(25)$ [49] is the weak axial coupling constant.

For first-forbidden transitions the shape factor reads

$$C(W) = k + kaW + kb/W + kcW^2. \tag{10}$$

where the factors k,ka,kb and kc are defined as [50]

$$\begin{aligned} k = {} & \left[\zeta_0^2 + \tfrac{1}{9} w^2\right]_{(0)} + \left[\zeta_1^2 + \tfrac{1}{9}(x+u)^2 - \tfrac{4}{9}\mu_1\gamma_1 u(x+u)\right. \\ & \left. + \tfrac{1}{18} W_0^2 (2x+u)^2 - \tfrac{1}{18}\lambda_2 (2x-u)^2\right]_{(1)} \\ & + \left[\tfrac{1}{12} z^2 \left(W_0^2 - \lambda_2\right)\right]_{(2)}, \end{aligned} \tag{11a}$$

$$ka = \left[-\tfrac{4}{3} uY - \tfrac{1}{9} W_0 (4x^2 + 5u^2)\right]_{(1)} - \left[\tfrac{1}{6} W_0 z^2\right]_{(2)}, \tag{11b}$$

$$kb = \tfrac{2}{3}\mu_1\gamma_1 \{-[\zeta_0 w]_{(0)} + [\zeta_1 (x+u)]_{(1)}\}, \tag{11c}$$

$$\begin{aligned} kc = {} & \tfrac{1}{18}[8u^2 + (2x+u)^2 + \lambda_2 (2x-u)^2]_{(1)} \\ & + \tfrac{1}{12}[(1+\lambda_2) z^2]_{(2)}, \end{aligned} \tag{11d}$$

with

$$\begin{aligned} V = \xi' v + \xi w', \quad \zeta_0 = V + \frac{1}{3} w W_0, \\ Y = \xi' y - \xi (u' + x'), \quad \zeta_1 = Y + \frac{1}{3}(u - x) W_0. \end{aligned} \tag{12}$$

The numbers in parenthesis after the closing brackets denote the rank of the operators inside. The parameter γ_1 is given by $\sqrt{1 - (\alpha Z)^2}$. For the Coulomb wave functions we use the approximations $\mu_1 \approx 1$ and $\lambda_2 \approx 1$ [51]. The quantity $\xi = \alpha Z/(2R)$, where we choose $R = \sqrt{\langle r \rangle^2}$.

In the Condon-Shortley phase convention [48] the matrix elements for β^- transitions are

$$w = -g_A \sqrt{3} \frac{\langle f \| \sum_k r_k \left[\boldsymbol{C}_1^k \otimes \boldsymbol{\sigma}^k\right]^0 \boldsymbol{t}_-^k \| i \rangle}{\sqrt{2J_i + 1}}, \tag{13a}$$

$$x = -\frac{\langle f \| \sum_k r_k \boldsymbol{C}_1^k \boldsymbol{t}_-^k \| i \rangle}{\sqrt{2J_i + 1}}, \tag{13b}$$

$$u = -g_A \sqrt{2} \frac{\langle f \| \sum_k r_k \left[\boldsymbol{C}_1^k \otimes \boldsymbol{\sigma}^k\right]^1 \boldsymbol{t}_-^k \| i \rangle}{\sqrt{2J_i + 1}}, \tag{13c}$$

$$z = 2 g_A \frac{\langle f \| \sum_k r_k \left[\boldsymbol{C}_1^k \otimes \boldsymbol{\sigma}^k\right]^2 \boldsymbol{t}_-^k \| i \rangle}{\sqrt{2J_i + 1}}, \tag{13d}$$

$$w' = -g_A \frac{2}{\sqrt{3}} \frac{\langle f \| \sum_k r_k I(1,1,1,1,r_k) \left[\boldsymbol{C}_1^k \otimes \boldsymbol{\sigma}^k\right]^0 \boldsymbol{t}_-^k \| i \rangle}{\sqrt{2J_i + 1}}, \tag{13e}$$

$$x' = -\frac{2}{3} \frac{\langle f \| \sum_k r_k I(1,1,1,1,r_k) \boldsymbol{C}_1^k \boldsymbol{t}_-^k \| i \rangle}{\sqrt{2J_i + 1}}, \tag{13f}$$

$$u' = -g_A \frac{2\sqrt{2}}{3} \frac{\langle f \| \sum_k r_k I(1,1,1,1,r_k) \left[\boldsymbol{C}_1^k \otimes \boldsymbol{\sigma}^k\right]^1 \boldsymbol{t}_-^k \| i \rangle}{\sqrt{2J_i + 1}}. \tag{13g}$$

The matrix elements connected with the relativistic corrections are

$$\xi' v = -g_A \frac{\langle f \| \sum_k \gamma_5^k \boldsymbol{t}_-^k \| i \rangle}{\sqrt{2J_i + 1}}, \tag{14a}$$

$$\xi' y = -\frac{\langle f \| \boldsymbol{\alpha}^k \boldsymbol{t}_-^k \| i \rangle}{\sqrt{2J_i + 1}}, \tag{14b}$$

with γ_5 and $\boldsymbol{\alpha}$ being the Dirac matrices. Due to the fact that our formalism is relativistic, we do not perform a nonrelativistic reduction in the evaluation of the matrix elements in Eqs. (14). The quantity $\boldsymbol{C}_{LM}$ equals

$$\boldsymbol{C}_{LM} = \sqrt{\frac{4\pi}{2L+1}} Y_{LM}, \tag{15}$$

where Y_{LM} are the spherical harmonics

As the matrix elements are independent of the electron and neutrino energies, the integrals over the electron phase space are evaluated independently and appear only as multiplicative factors. The function $I(1,1,1,1,r)$ takes into account the nuclear charge distribution, and in the approximation of the uniform spherical distribution it has the form [50]

$$I(1,1,1,1,r) = \frac{3}{2} \begin{cases} 1 - \frac{1}{5}\left(\frac{r}{R}\right)^2, & 0 \leqslant r \leqslant R, \\ \frac{R}{r} - \frac{1}{5}\left(\frac{R}{r}\right)^3, & r > R. \end{cases} \tag{16}$$

Systematic calculations of β-decay half-lives determined by Gamow-Teller transitions have shown that the theoretical matrix elements need to be quenched by a factor q, that has been found to be independent of the particular transition considered and is approximately constant over the nuclear chart [52,53]. It has also been shown that the results of a QRPA and shell model calculation for the neutrino-nucleus cross

sections are in very good agreement if the same quenching factor for the axial-vector coupling constant g_A is used [54]. There is also evidence that the total first-forbidden transition strength is overestimated by theoretical approaches. In addition, the quenching factor seems to depend on the model space used and on the particular first-forbidden operator [18,55–59]. So far no study has addressed the quenching of first-forbidden transitions of global calculations of β-decay half-lives. In two recent studies, the particle-vibration coupling model was used to describe Gamow-Teller and spin-dipole excitations in ^{208}Pb [60,61]. Both show that, compared to the RPA results, the predicted strength is fragmented and reduced by similar amounts, indicating that using a single quenching factor for all transitions is justified. In our calculations, we account for the quenching of both the Gamow-Teller and first-forbidden transitions by using the same effective value of $g_A = -1.0$.

III. RESULTS

A. β-decay half-lives

In Fig. 2 we compare the calculated half-lives for four isotopic chains, including both the even and odd atomic numbers, where the half-lives are obtained from the decay rate in Eq. (7):

$$T_{1/2} = \frac{\ln 2}{\lambda}. \tag{17}$$

In the four panels we show a comparison of the present results with the data and the FRDM results for the strontium (Sr, $Z = 38$), yttrium (Y, $Z = 39$), silver (Ag, $Z = 47$), and cadmium (Cd, $Z = 48$) isotopic chains. The two lightest isotopic chains, strontium and yttrium, are found between two closed proton shells $Z = 28$ and $Z = 50$. Our calculation has difficulties reproducing the half-lives of the longest lived nuclei due to the rather low Q values; however, for isotopes more neutron-rich than $N = 58$ we obtain very good agreement with the data, with a slight tendency to underestimate the half-lives of yttrium isotopes. The FRDM+QRPA approach displays erratic jumps in the half-lives and odd-even staggering that is not present in the data. For very neutron-rich isotopes the two models provide very similar results due to the increase of Q_β values.

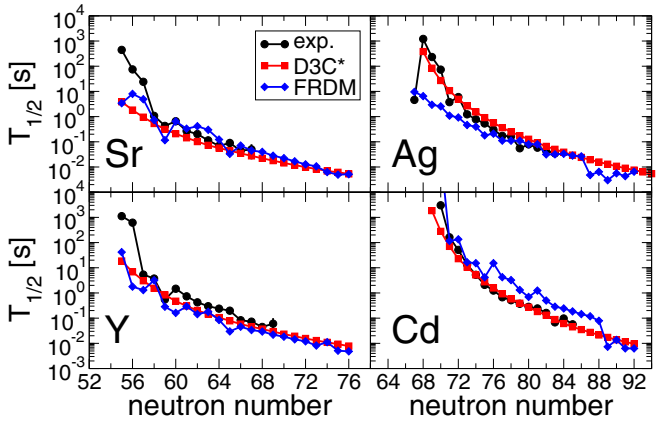

FIG. 2. Comparison of the calculated half-lives with the FRDM results and the experimental data for the strontium (upper left), yttrium (lower left), silver (upper right), and cadmium (lower right) isotopic chains. In cases where they are not visible, the error bars are smaller than the data marker.

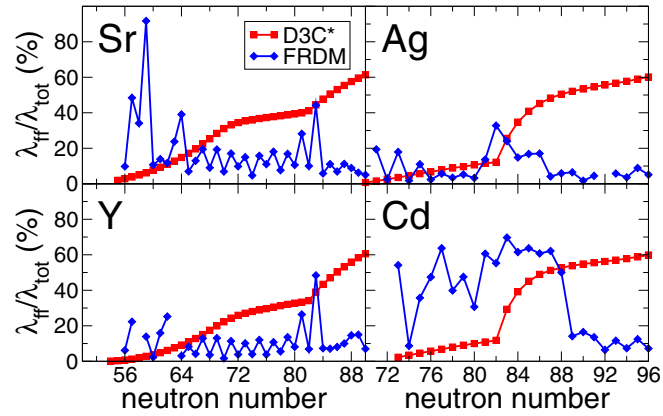

FIG. 3. Percentage of first-forbidden transitions contributing to the decay of Sr, Y, Ag, and Cd isotopes. In the cases where it was not possible to extract the value for a particular model, the data point was not plotted.

The right panels compare the present calculation and the FRDM+QRPA model with data for nuclei close to the $Z = 50$ closed proton shell, including the silver and cadmium isotopic chains. Similar to the two lighter isotopic chains, the D3C* interaction provides an excellent description of the decay properties of neutron-rich nuclei, with the results correctly following the trend along the chain. In the case of silver, the present work reproduces the trend quite well in comparison with the FRDM. Most likely, because the FRDM reproduces the half-life of ^{114}Ag it cannot provide a good trend for most of the isotopic chain. The half-life of this nucleus is uncharacteristically short compared with the surrounding isotopes due to the $J^\pi = 1^+$ angular momentum and parity of the ground state, which quickly decays into the 0^+ ground state of ^{114}Cd. For cadmium nuclei both models do quite well, although the FRDM shows unexpected changes in the half-lives along the chain, as in the cases of other elements.

In the following figure, Fig. 3, we plot a comparison of the contribution of the first-forbidden transitions in the total decay rate, in percent, between the two models. For the FRDM, we have extracted the values by comparing the results of Refs. [62] and [19]. Due to the changes in the details of the calculation between the two publications, the values presented here are not precise. We expect them to be a good qualitative measure of the actual values. The FRDM calculation predicts, in two out of four isotopic chains, a large contribution (more than 50%) of first-forbidden transitions in nuclei close to stability, and a decrease in more neutron-rich nuclei. For nuclei in the isotopic chains of yttrium and silver, FRDM predicts a steady, small contribution below 20% for most of the nuclei, with odd-even staggering.

The present results predict a rather small contribution of the forbidden transitions in nuclei close to stability, with a

smooth increase with additional neutrons. This increase is particularly visible at the $N = 82$ neutron shell closures for Ag and Cd isotopes, where the neutrons begin to occupy the $2f_{7/2}$ and the $1h_{9/2}$ orbits, enabling the strong $\nu 2f_{7/2} \rightarrow \pi 1g_{7/2}$ and $\nu 1h_{9/2} \rightarrow \pi 1g_{9/2}$ transitions, which significantly increase the contribution of the first-forbidden transitions, as these transitions appear at low excitation energies in the daughter nucleus. In the two lighter isotopic chains, the contribution is negligible for the lightest isotopes and increases smoothly up to $\approx 30\%$ where it reaches a plateau. The main difference in the transitions between, e.g., ^{94}Sr and ^{114}Sr is the occupied neutron $2d_{3/2}$ state, which contributes to the total rate by decaying to the proton $2p$ states. Above the $N = 82$ closed neutron shell, the contribution of the first-forbidden transitions again rises with the occupation of the $2f_{7/2}$ and the $1h_{9/2}$ states, just as in the silver and cadmium isotopes.

As discussed above, our calculations are only strictly applicable to even-even nuclei. However, we have extended them to odd-A and odd-odd nuclei in order to provide a complete coverage for r-process simulations. Our approach cannot account for mismatches between the angular momenta of the ground states of parent and daughter nucleus in the decay. However, this aspect becomes less and less important as the Q value for the decay increases. This is one of the reasons why our approach becomes better as we move far from stability. Our predictions for half-lives are certainly not worse than those computed by the FRDM+QRPA approach [19] that is currently the standard model for half-lives used in r-process simulations. We will discuss this aspect in more detail in the next section.

It is also possible to compare the present results with the newest data available to assess the quality of the extrapolation of half-lives into currently inaccessible regions. Figure 4 compares our calculations with the recently measured β-decay half-lives [9] for a number of isotopic chains with atomic number in the range $36 \leqslant Z \leqslant 43$. The results obtained with the D3C* interaction are in agreement with the experiment within a factor 2. The FRDM+QRPA approach, on the other

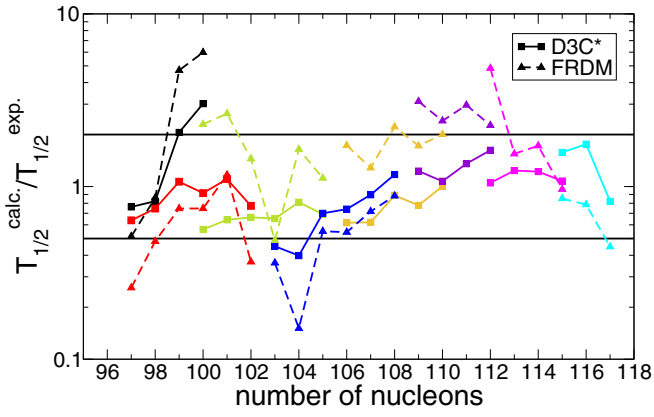

FIG. 4. The ratio of the calculated and measured half-lives for nuclei in the $36 \leqslant Z \leqslant 43$ isotopic chains from Ref. [9], for the D3C* interaction (full line) and the FRDM (dashed line). Different colors denote the isotopic chains, while the thick black lines denote deviations by a factor 2.

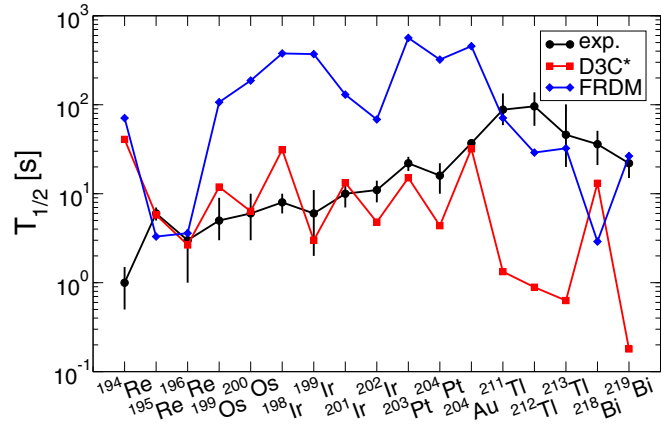

FIG. 5. Comparison of the data (denoted with black circles) with the results of the present work (red squares) and the FRDM (blue diamonds).

hand, tends to predict too long half-lives and displays jumps in the ratio for specific nuclei.

As we move to heavier nuclei both models have significant difficulties while attempting to reproduce the recent data. Figure 5 compares the two models with measurements [12,13]. FRDM significantly overestimates the half-lives of most of the nuclei, by more than an order of magnitude. It is only for nuclei around the $Z = 82$ closed proton shell that it provides a reasonable description of the data. An interesting effect occurs in the case of rhenium isotopes, where the half-life of ^{194}Re is overestimated, but half-lives of the two heavier isotopes are reproduced. The discrepancy seems to be related to the change of prolate to oblate deformation in moving from ^{194}Re to the heavier isotopes [38]. With the exception of ^{194}Re, the D3C* calculations reproduce all β-decay half-lives of the $Z \leqslant 79$ nuclei shown in Fig. 5 within an order of magnitude. Larger differences appear for heavier nuclei. Taking into account that the nuclei shown in Fig. 5 have half-lives in the range 1 to 100 s, one should conclude that both FRDM and D3C* approaches provide a fair reproduction of data. Certainly, the agreement is worse that the one obtained in Fig. 4, but this should not be consider as a drawback of the two models discussed to reproduce half-lives of heavier nuclei. It simply reflects the fact that, for heavy nuclei, the half-lives are only known for relatively long-lived nuclei close to stability that normally have small Q_β decay windows. The theoretical description of these decays is a challenge for any theoretical model as the decay rate depends on very few selected transitions.

Finally, in Fig. 6 we compare the theoretical results with the very recent measurement of half-lives of 110 neutron-rich isotopes, 40 of which have not been previously measured. In the upper panel we plot the results of the present study, from the isotopes of rubidium to tin, and from $N = 65$ to $N = 89$. Almost all of the values can be found within a factor of 2 from the data, with very little scatter for different isotopic chains, except for the case of tin where we underestimate the half-lives by a factor of 5. Within a particular chain the data is reproduced smoothly, with very weak odd-even staggering. In the case of

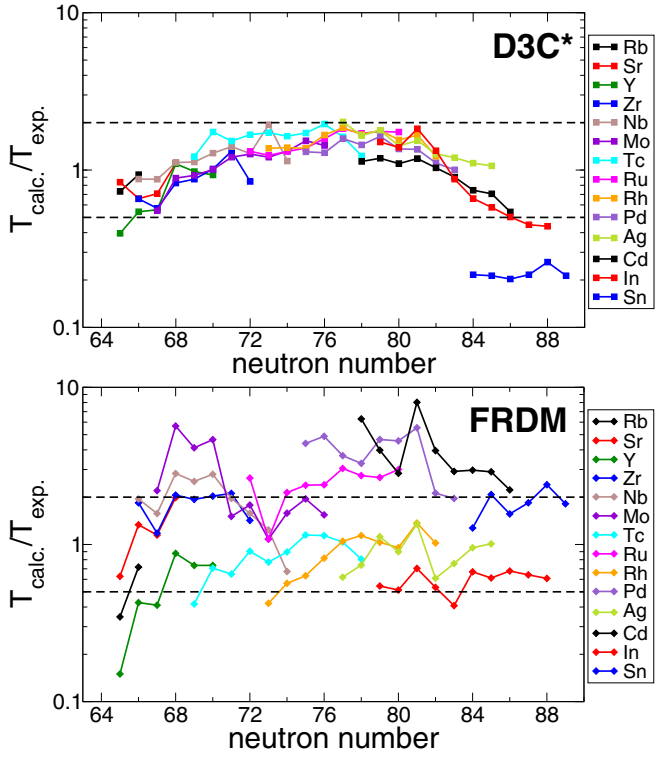

FIG. 6. The ratio of the calculated and experimental half-lives for the recently measured 110 isotopes [63]. In the top panel we present the results obtained in the present study, while in the bottom panel we present the FRDM results [19].

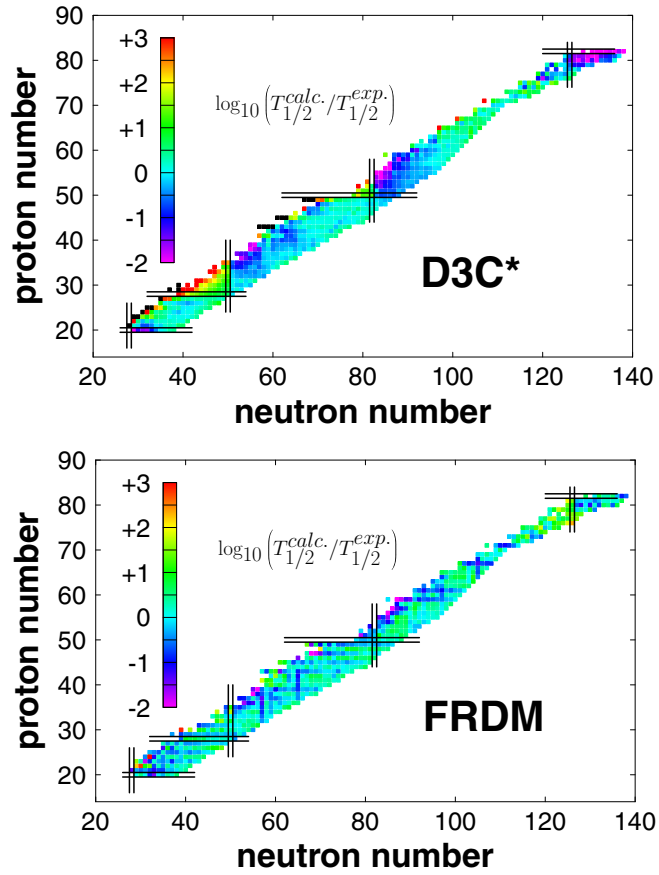

FIG. 7. The logarithm of the ratio of the calculated and experimental half-lives is plotted for all neutron-rich nuclei with available data, with half-lives shorter than 1 hour. Black squares indicate that the model did not provide a finite half-life. In the top panel we plot the results of the present study, while in the bottom panel we plot the ratios obtained with the FRDM.

FRDM the scatter is much larger, and we also observe some regularities. The half-lives of nuclei in isotopic chains with an even atomic number are systematically overestimated by a factor of 2 or more; these are the Zr, Mo, Ru, Pd, Cd, and Sn isotopes.

Figure 7 shows the ratio of the calculated and measured half-lives for neutron-rich nuclei with half-lives shorter than 1 hour. We show the results for the FRDM+QRPA approach and our own calculations (bottom and top panels, respectively). The present calculation has difficulties in reproducing the half-lives for nuclei close to simultaneous neutron and proton shell closure. In particular, the greatest discrepancies appear in the regions "northwest" of the doubly closed nuclei ^{78}Ni and ^{132}Sn. The amount of low energy GT strength for such nuclei is very sensitive to correlations [18] that are not captured by the QRPA approach. For an improved description of the low-energy strength distributions of these nuclei, complex configurations need to be included to shift the transition strength from the GT resonance to low energies [60,61]. Coupling to collective phonon excitations is known to have a strong impact on the single particle structure around shell closures [64], and will enhance the decay rate of these nuclei [65].

There are also three regions where the D3C* calculations predicts shorter decay half-lives, i.e., the regions around the ^{90}Kr($Z = 36$, $N = 54$) and ^{140}Ba ($Z = 56$, $N = 84$) nuclei, and the $Z \lesssim 82\, N > 126$ region. The first two cases correspond to regions of low deformation [66]. However, there are indications that nuclei in that region are gamma soft [67,68]. So far the impact of gamma-softness on β-decay rates has not been explored. It is interesting that the FRDM+QRPA approach also predicts shorter half-lives for these two regions. In the case of the region $Z \lesssim 82\, N > 126$, we are dealing with nuclei with half-lives longer than 100 s. The decay rate is determined by few transitions that depend very sensitively on the predicted single-particle structure. In particular, for Hg and Tl isotopes, above the $N = 126$ closed neutron shell the decay is dominated by the Gamow-Teller $\nu 1i_{11/2} \rightarrow \pi 1i_{13/2}$ and the $1^- \nu 1i_{11/2} \rightarrow \pi 1h_{9/2}$ configurations. These transitions are not possible for isotopes with $N \leqslant 126$, but above the neutron shell closure the $\nu i_{11/2}$ becomes significantly occupied (occupation probability is already $\approx$0.2 for ^{210}Hg and ^{211}Tl) at an energy of $E_{i_{11/2}} \approx -2.5$ MeV.

Figure 8 shows the ratio of the calculated and the experimental half-lives versus the experimental half-life. Different symbols are used for even-even, the odd-N, odd-Z, and the odd-odd nuclei. The data are taken from Ref. [37]. For long-lived nuclei we observe a very large spread of the ratios due to the high sensitivity of the decay rate to the details of the low energy transition strength. Short-lived nuclei have

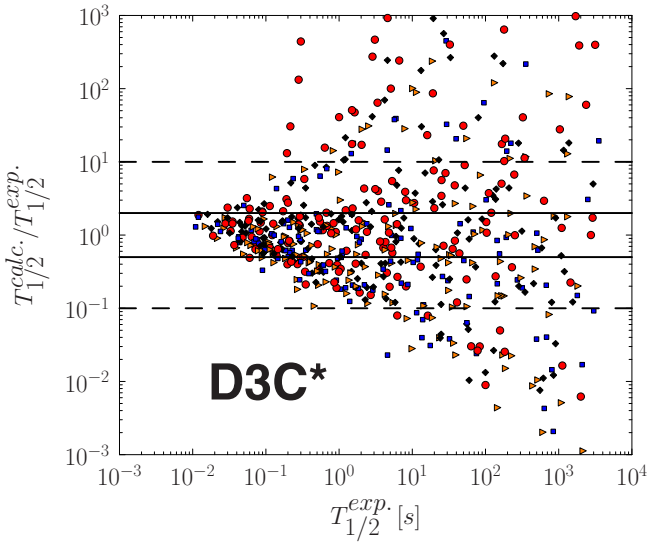

FIG. 8. The ratio of the calculated and the experimental half-lives [37] versus the experimental half-life. Different types of nuclei are denoted with different symbols. Even-even nuclei are denoted with blue squares, odd-N with orange triangles, odd-Z with black diamonds, and odd-odd nuclei are denoted with red circles.

large Q values, and generally several transitions contribute to the decay rate. This makes these nuclei less sensitive to the detailed position and strength of particular transitions. Our results show that the ratio of half-lives converges towards 1 with decreasing half-life, for even-even, odd-A, and odd-odd nuclei equally. This behavior points to the reliability of the model for all types of nuclei taking part in the r process, as almost all of the predictions lie within an order of magnitude from the data, with a large majority within a factor of 2.

In Table I we provide a quantitative analysis of the results, by using several measures of the model precision. Because both the observable (half-life) and the ratio of the calculated and experimental values span orders of magnitude, we define r_i as the logarithm of the ratio of calculated and experimental half-lives,

$$r_i = \log_{10} \frac{T^{\text{calc.}}_{1/2}}{T^{\text{exp.}}_{1/2}}, \tag{18}$$

with the average value of the ratio providing a measure of the global deviation from experimental values,

$$\bar{r} = \frac{1}{N} \sum_{i=1}^{N} r_i, \tag{19}$$

while the standard deviation provides a measure of the spread [69],

$$\sigma = \left[\frac{1}{N} \sum_{i=1}^{N} (r_i - \bar{r})^2 \right]^{1/2}. \tag{20}$$

The average deviation and the spread obtained using the D3C* and the finite-range droplet model [19] are shown. The top part of the table provides data for nuclei with the experimental half-life shorter than a particular value. The average value of deviation from experiment $\bar{r}$ is comparable between the two models. There are small differences for particular sets of nuclei, but they are not significant. The resulting standard deviation is larger with the D3C* for long-lived nuclei, confirming that the description of nuclei with small Q_β values is challenging for the model. For nuclei with half-lives shorter than 1 s, the models are comparable both in the average and the standard deviation, and for even less stable nuclei D3C* even manages to provide a smaller spread of ratios.

TABLE I. Comparison of the average deviations [Eq. (19)] and their standard deviations [Eq. (20)] between the model used in the present work and the FRDM. In the upper part of the table, we show the results structured with respect to the experimental half-life of the nuclei included, while in the lower part of the table we show the results for nuclei with half-lives shorter than 1 s, but separated into groups of even-even, odd-Z, odd-N, and odd-odd nuclei.

	D3C*		FRDM	
	$\bar{r}$	σ	$\bar{r}$	σ
$T_{\text{exp.}}$				
<1000 s	0.011	0.889	0.021	0.660
<100 s	0.057	0.791	0.040	0.580
<10 s	0.061	0.645	0.046	0.515
<1 s	0.011	0.436	0.019	0.409
<0.1 s	0.041	0.195	0.021	0.354
Nucleus type				
even-even	−0.037	0.331	0.333	0.226
odd-Z	0.054	0.328	−0.128	0.288
odd-N	−0.086	0.387	0.124	0.436
odd-odd	0.089	0.582	−0.179	0.409
total	0.011	0.436	0.019	0.409

In the bottom part of the table we provide the results, including nuclei with the experimental half-life lower or equal to 1 s, but shown for each type of nuclei, i.e., even-even, odd-Z, odd-N, and odd-odd, separately. From this point of view, the results of the two models are significantly different. In the present work, the half-lives of even-even and odd-N nuclei are somewhat underestimated by roughly 10%–20%, and the half-lives of odd-Z and odd-odd nuclei are, on average, overestimated by 15% and 20%, respectively. These results agree with the assumption that the model is capable of describing all types of nuclei equally well, as the half-lives of odd-A and odd-odd nuclei are reproduced as well as half-lives of even-even nuclei. The difference between various types of nuclei becomes more evident by looking at the standard deviations. Here, the spread of values for even-even and odd-A nuclei is comparable, but the standard deviation of the results for odd-odd nuclei is almost twice as large, pointing to potential angular momentum issues in the ground state of an odd-odd nucleus. It is interesting that our model does particularly well for even-N nuclei that are the most relevant nuclei for r-process nucleosynthesis, as these nuclei are favored by neutron-captures.

The FRDM+QRPA half-lives show a distinctly different behavior. As opposed to the D3C* model, the FRDM overestimates the half-lives of even-even and odd-N nuclei, by a factor

of 2.15 and 1.33, respectively. That the predicted half-lives of even-even nuclei are on average twice the experimental value is surprising because, similarly to our calculation, the model should be more suitable for these nuclei. This fact may have important consequences for r-process nucleosynthesis and might be responsible for the differences in r-process nucleosynthesis discussed on Sec. III D. However, waiting-point nuclei also include odd-Z and even-N nuclei, and in both models there is a cancellation between even-even and odd-Z nuclei.

On the other hand, the half-lives of odd-Z and odd-odd nuclei are underestimated by approximately 30% and 50%, respectively. The standard deviations are comparable between the two models for odd-A nuclei, but are smaller for even-even and especially for odd-odd nuclei. Still, for both models the odd-N and odd-odd nuclei are the most difficult to describe and result in the largest spreads. So, even though the average $\bar{r}$ of the FRDM is close to zero, it is actually a result of the cancellation of overestimated and underestimated half-lives in different types of nuclei. This behavior has also appeared in previous evaluations of the β-decay rates (see Ref. [62], Table B), where the half-lives of short-lived even-even nuclei were, on average, overestimated by almost a factor of 4, while the half-lives of odd-A and odd-odd nuclei were underestimated by a factor of 2. In comparison, the results of the present work are more consistently close to reproducing the data, even though the larger standard deviations highlight some unresolved issues.

Finally, in Fig. 9 we plot the ratio of half-lives obtained in the present study with the FRDM half-lives [19]. For light and medium-heavy nuclei, the results are quite similar. Close to the valley of stability, the D3C* model tends to provide longer half-lives than the FRDM for particular nuclei, especially so in the regions "northwest" of the doubly closed nuclei ^{78}Ni and ^{132}Sn. Farther from the valley of stability the two models provide comparable results, with the difference that the present calculation predicts smoother increase in the decay rates. For very heavy nuclei with $N > 126$, however, the present study predicts half-lives to be shorter, by more than an order of magnitude, than the FRDM predictions. This is especially clear in nuclei with high atomic numbers, i.e., $Z \gtrapprox 95$ where the difference is as large as three orders of magnitude. This may have significant consequences on the dynamics of the r-process nucleosynthesis in neutron star merger conditions [70].

B. Impact of first-forbidden transitions

The results presented in this manuscript are the first global calculations of β-decay half-lives for neutron-rich nuclei that treat Gamow-Teller and first-forbidden transitions on an equal footing. In this section, we provide a detailed analysis on the impact of first-forbidden transitions, with particular focus on nuclei with magic neutron numbers $N = 50$, 82, and 126 that have been the subject of many theoretical calculations. Additionally, for $N = 50$ and 82, experimental data is available that has contributed to constrain the calculations.

Figure 10 compares the β-decay half-lives for r-process nuclei with neutron magic numbers $N = 50$, 82, and 126 with the FRDM+QRPA model [19], the shell-model calculations of Ref. [18], and data [37]. For the $N = 50$ isotones (upper panel) with $Z \geqslant 28$ the present calculations fail to reproduce the measured half-lives. In these nuclei the $f_{7/2}$ proton shell is fully occupied, suppressing low energy Gamow-Teller transitions. The decay consequently proceeds mainly by first-forbidden transitions, resulting in long decay half-lives. As a consequence, the model predicts a large contribution of forbidden transitions to the decay rate (see Fig. 11). This is probably a limitation of the QRPA type calculations that are not able to produce enough correlations around the proton magic number $Z = 28$. This problem does not seem to be present in the FRDM+QRPA approach. However, one should keep in mind that in this approach the Gamow-Teller and first-forbidden contributions are not derived based on the same

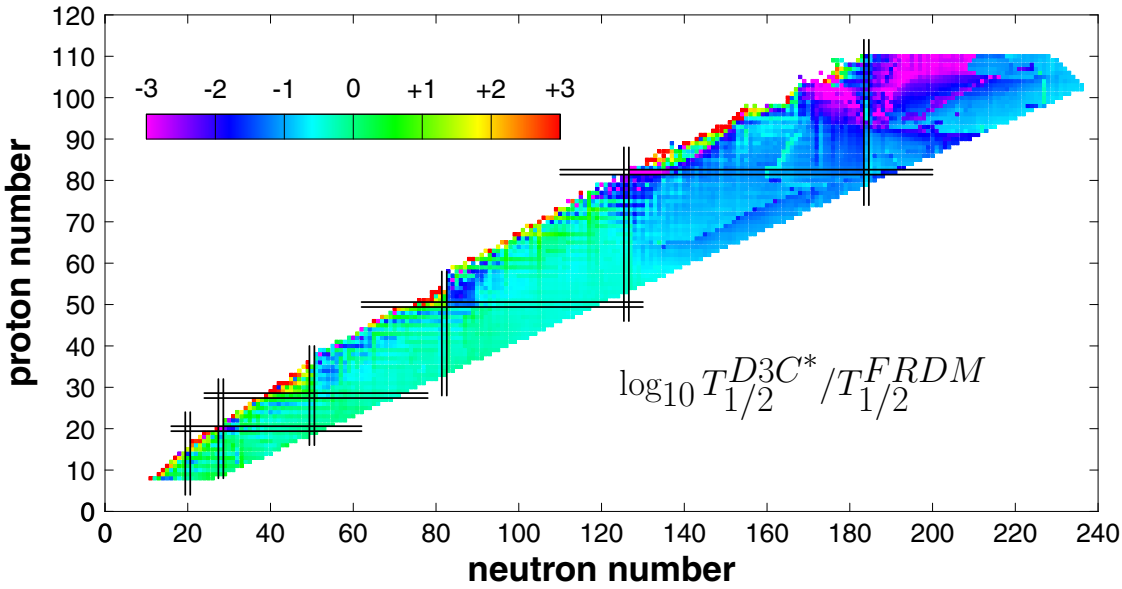

FIG. 9. Ratio of half-lives computed in the present manuscript to those based on the FRDM+QRPA approach [19]. Black lines indicate the position of (predicted) closed proton and neutron shells.

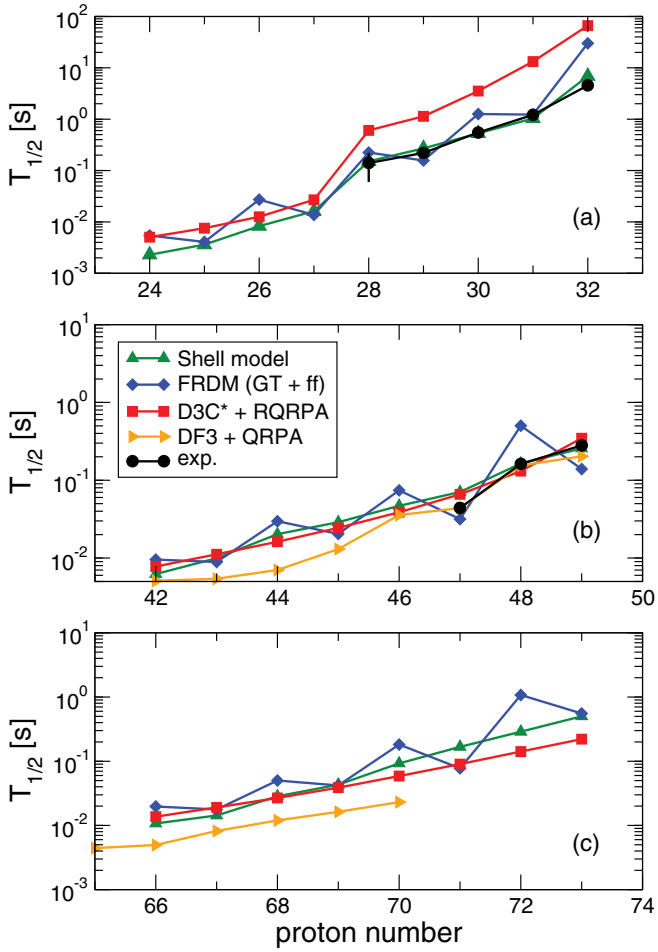

FIG. 10. β-decay half-lives for $N = 50$ (a), $N = 82$ (b), and $N = 126$ (c) isotopic chains. The present results are compared with those of FRDM [19], the shell-model [18], DF3 [27], and data [37].

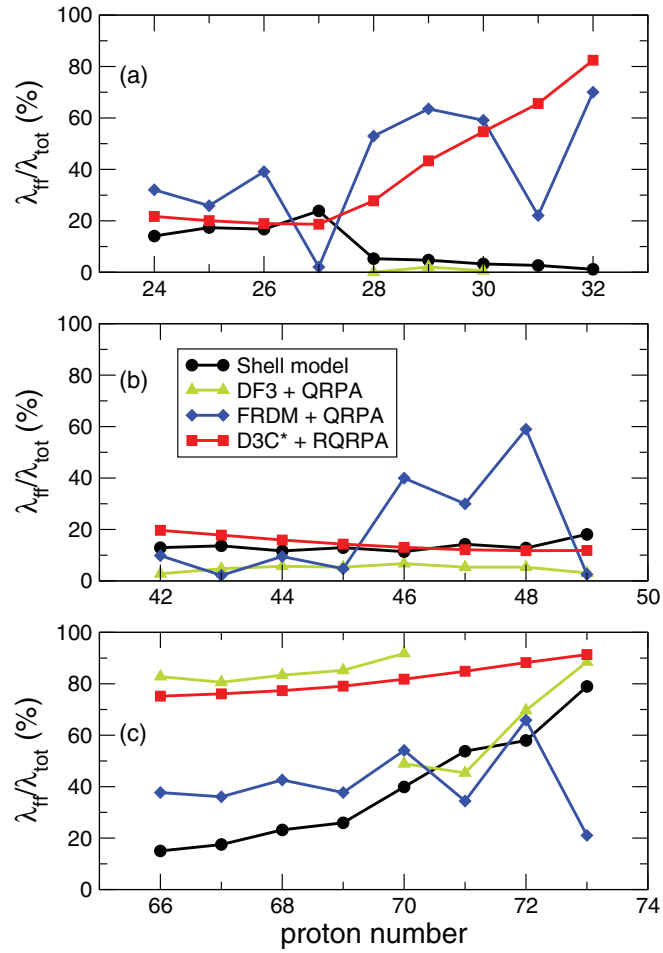

FIG. 11. The contribution of the first-forbidden transitions in the total decay rate for the $N = 50$, $N = 82$, and $N = 126$ isotonic chains, in the top, central and bottom panels, respectively. Present results, denoted with black squares, are compared with the FRDM calculation [19] (denoted with green triangles), DF3 calculation [20] (denoted with blue diamonds), and a recent shell model calculation [18] (denoted with red circles).

microscopic model. As discussed above, the FRDM+QRPA approach tends to produce strong odd-even effects that are not present in the data or in the other approaches.

The situation is different for the $N = 82$ and $N = 126$ isotonic chains. In these nuclei there is no proton shell closure that hinders low energy Gamow-Teller transitions, and in principle both Gamow-Teller and forbidden transitions are possible. The present study predicts a very similar contribution of first-forbidden transitions to the shell model, $\sim 20\%$, for all the $N = 82$ isotones. FRDM+QRPA predicts rather large forbidden contributions for $Z = 46,47,48$ and similar values for the other isotones. The odd-even staggering present in the β-decay half-lives is also manifested on the contribution of forbidden transitions. For $N = 126$ all models predict an enhanced contribution of forbidden transitions. Reference [18] argues that the contribution of forbidden transition should decrease with decreasing proton number. This reduces the number of protons in the $h_{11/2}$ increasing the role of $\nu h_{9/2} \rightarrow \pi h_{11/2}$ Gamow-Teller transitions. While all models predict such a reduction, the magnitude varies from model to model. The present calculations predict a relatively minor reduction from 90% at $Z = 73$ to 70% at $Z = 66$, while the shell-model predicts a much larger reduction reaching below 20% at $Z = 66$. Experimental data will be very important to further constrain the theoretical calculations.

Figure 12 shows the contribution of β-decay half-lives for all nuclei with predicted β-decay half-lives shorter than 1 s. In general, first-forbidden transitions do not noticeably impact the total decay rate in nuclei close to the valley of stability with $Z \leqslant 50$. Here, protons and neutrons fill orbits with the same parity, and the decay is dominated by Gamow-Teller transitions. It is interesting to notice the similar behavior for nuclei located around ^{78}Ni and ^{132}Sn. Moving in the "southwest" direction ($Z < 28$, $N < 50$ and $Z < 50$, $N < 82$ respectively) forbidden transitions are initially suppressed. However, once protons start to occupy orbits with different parity ($Z < 20$ or $Z \lesssim 40$) the contribution of forbidden transitions grows to values of 40% to 60% depending on the detailed nuclear structure. Moving in the "east" direction ($N > 50$ and $N > 82$ respectively), we see that the contribution of forbidden transitions is rather independent of the charge number and does not vary when crossing the proton shell

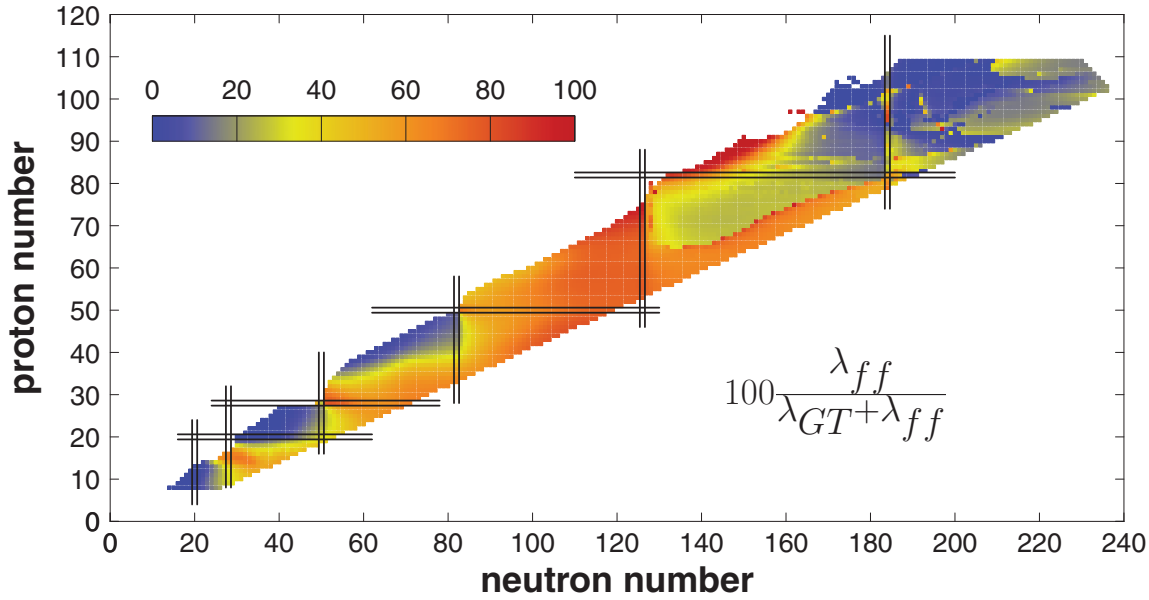

FIG. 12. The contribution of the first-forbidden transitions in the total decay rate for nuclei with predicted half-lives shorter than 1 s. Black lines indicate the positions of (predicted) closed proton and neutron shells.

closure at $Z = 28$ and $Z = 50$, respectively. In these regions, for neutrons and protons there are valence orbits with both positive and negative parity, and consequently Gamow-Teller and forbidden transitions contribute in similar amounts to the decay. The situation is different in the region between $N = 50$ and $N = 82$. Here, once protons completely fill the pf shell ($Z > 40$), forbidden transitions are suppressed and the decay is dominated by Gamow-Teller transitions.

An interesting phenomena occurs once we move to nuclei with $N > 126$ with a clearer manifestation once we reach $N = 184$. For these nuclei, neutrons and protons occupy orbits that differ in two units of the main oscillator quantum number, $\mathcal{N} = 2n + l$. Under the assumption of isospin symmetry the single-particle orbits for neutrons and protons will be identical, and consequently Gamow-Teller transitions will be exactly zero. However, due to isospin breaking mainly due to the Coulomb interaction the proton and neutron single-particle states are not identical allowing for Gamow-Teller transitions, even if somewhat suppressed. This is the reason why forbidden transitions dominate in this whole region with GT transitions representing around 20% of the decay rate.

C. β-delayed neutron emission

β-delayed neutron emission probabilities are another component in the late stages of r-process nucleosynthesis. Here we approximate the probability of emission of x neutrons as the ratio of the rates between S_{xn} and $S_{(x+1)n}$ separation energies to the total decay rate, i.e.,

$$P_{xn} = \frac{\sum_{i,E_i=S_{xn}}^{\min(Q_\beta,S_{(x+1)n})} \lambda_i}{\sum_i \lambda_i}. \quad (21)$$

This is a relatively crude approximation, where the nucleus always emits as many neutrons as energetically possible. Thus, the predicted average number of emitted neutrons is invariably overestimated. Neutron emission probabilities are, therefore, very sensitive to the neutron separation energies and display strong odd-even effects. As mean-field models cannot reproduce this staggering, we employed the global nuclear mass model [66] to obtain the neutron separation energies. Additionally, only for the purpose of calculating the emission probabilities, we smeared the β strength distributions with a Lorentzian in order to reduce the sensitivity of the neutron emission probabilities to the positions of particular transitions. The width of the Lorentzian was determined by calculating the average number of delayed neutrons emitted by the fission fragments of ^{235}U, $\langle n\rangle = 0.0158 \pm 0.0005$ [71]. In this way the width was adjusted to $\Gamma = 65$ keV. From the probabilities, we obtain the average number of emitted neutrons after the decay of a nucleus as

$$\langle n\rangle = \sum_i i\, P_{\text{in}}. \quad (22)$$

With this adjustment we can reproduce averaged emission probabilities with reasonable accuracy, especially in the context of heavy element nucleosynthesis where the β-delayed neutron emission is not the primary generator of uncertainties. Other approaches to the problem would include phenomenological models such as the one by Miernik [72,73], but at the cost of self-consistency of the model.

In Fig. 13 we plot the average number of emitted neutrons for neutron-rich nuclei included in this study. Close to the valley of stability, the Q values are smaller than the one neutron separation energies, making it impossible for the daughter nucleus to deexcite via neutron emission. With additional neutrons both the Q value increases and the separation energies decrease enabling the emission of one, two, or more neutrons

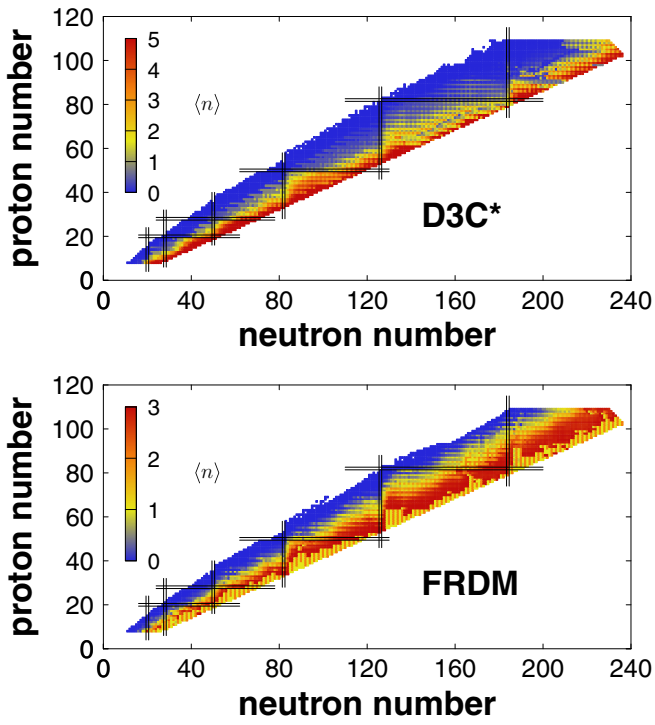

FIG. 13. Average number of emitted neutrons after β decay calculated with the FRDM and the D3C* model. Note that because the available FRDM results only contain the emission probabilities for up to three neutrons emitted, and in the present work the probabilities are obtained for up to five emitted neutrons, the color scales are different.

after decay. This is particularly evident above neutron shell closures where the average number of emitted neutrons increases due to a drop in the separation energies. Another characteristic feature of $\langle n \rangle$ is the odd-even staggering as a function of atomic number. Isotopic chains with an even number of protons typically have a smaller average number of emitted neutrons, i.e., smaller probabilities of emitting more neutrons, than their odd-proton neighboring chains, which mimics the behavior of the Q values. A smaller odd-even staggering is also present within any isotopic chain, as a consequence of the staggering of the neutron separation energies.

While both the D3C* and the FRDM reproduce these general features, in other aspects there are significant differences. First, the FRDM evaluation was limited to a maximum of three emitted neutrons per decay, while the present study takes into account the possibility for up to five neutrons to be emitted in a decay. While there are no measurements which have observed five emitted neutrons after β decay, the nuclei we consider in this study are much more neutron-rich than those that can be created in current experimental facilities. The neutron separation energies are very small and the decay Q values very large, and the emission of a larger number of neutrons is energetically allowed. The results of the calculation confirm our predictions, as we obtain a finite probability of five neutron emission in nuclei with extreme values of the neutron-to-proton ratio. The consequence of this change is evident in very neutron-rich nuclei where the neutron separation energies are very small, and where the D3C* model predicts a larger average number of emitted neutrons which continuously increases up to the drip line, while the FRDM predicts a saturation of $\langle n \rangle$. On the other hand, for isotopes closer to stability the D3C* model predicts smaller vales of $\langle n \rangle$ and a more gradual increase toward the neutron drip line. Finally, in very neutron-rich nuclei the FRDM displays decidedly unphysical, sudden oscillations between the values of $\langle n \rangle = 1$ and $\langle n \rangle = 2$, while the present study predicts a smooth increase with the neutron number.

D. Consequences for heavy-element nucleosynthesis

To explore the impact of the obtained results on heavy element nucleosynthesis, we have performed r-process nucleosynthesis calculations based on the "hot" and "cold" r-process conditions from Ref. [3]. In the "hot" r-process scenario the r-process evolves under an $(n,\gamma) \rightleftarrows (\gamma,n)$ equilibrium that breaks down once the r-process freeze-out is reached. For the "cold" r-process scenario the evolutions proceeds by a competition between neutron captures and β decays. The neutron capture and photodissociation rates used on the network calculations are based on the statistical model approach [74] using the FRDM mass model [38]. The only difference between the calculations is the use of the FRDM+QRPA β-decay half-lives and β-delayed neutron emission probabilities [19] or those computed in the present study.

In Fig. 14, we compare the abundances obtained with the two models after the r process has ended. One can notice important differences, particularly in the region of the third r-process peak, $A \sim 195$, between the calculations. There are also differences in the abundances around the second peak, but the astrophysical conditions explored by the present trajectories are expected to contribute mainly to the third r-process peak region [3].

To get further insight into the origin of the differences in the abundances, we show in Fig. 15 the evolution of the neutron-to-seed ratio. Clearly, the D3C* half-lives result in an earlier r-process freeze-out, defined as the moment when the neutron-to-seed ratio reaches a value of 1. In Fig. 16, we plot the abundance patterns obtained with the new decay half-lives, for both the hot and cold trajectories, at the r-process freeze-out. At this moment, the two models predict very similar abundance patterns. Up to this point in time differences in β-delayed neutron emission had little impact in shaping the abundances. Their differences originate mainly in the β-decay rates.

To illustrate this point, Fig. 17 shows the average isotopic lifetimes at the freeze-out for the different calculations. It is expected that for both for the hot and cold r-process conditions, the r process has reached β-flow equilibrium by the freeze-out time [3]. Under these conditions the product of the average β-decay rate times the abundance for each isotopic chain is constant, i.e., $\lambda_\beta(Z)Y(Z) = \text{constant}$, with $Y(Z) = \sum_A Y(Z,A)$ and

$$\lambda_\beta(Z) = \frac{1}{\tau_\beta(Z)} = \frac{1}{Y(Z)} \sum_A \lambda_\beta(Z,A) Y(Z,A). \qquad (23)$$

This means that the isotopic abundances, $Y(Z)$, are proportional to the lifetime, $\tau(Z)$, and the material accumulates in

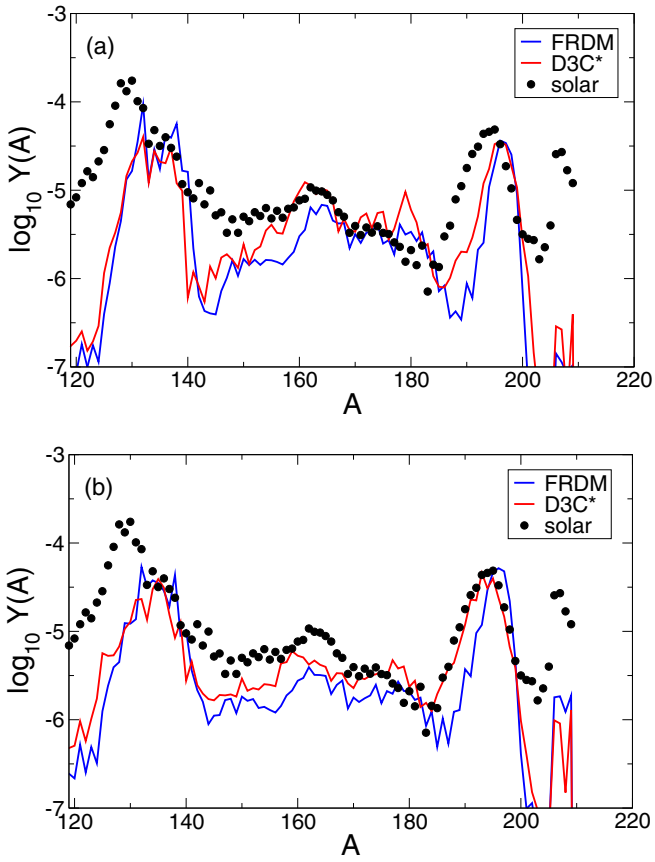

FIG. 14. The abundances of heavy nuclei resulting from a hot r-process (upper panel) or a cold r-process (lower panel) calculation using the half-lives obtained from the FRDM and the current model. The abundances plotted are the final values, after the r process has finished. The solid circles denote the solar r-process abundances.

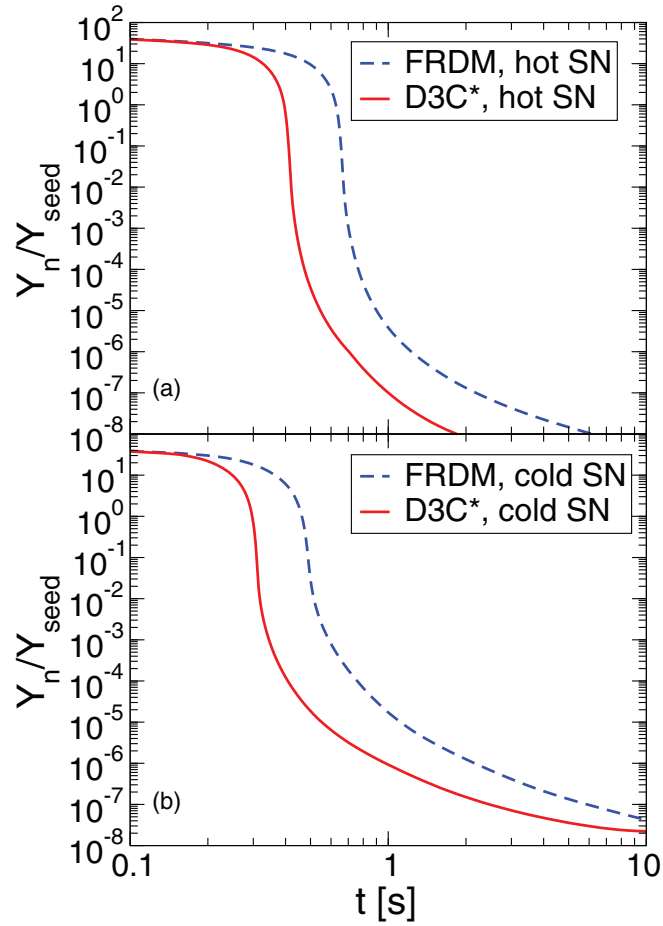

FIG. 15. The evolution of the neutron-to-seed ratio during the r process. The upper panel shows the results for the hot r process while the lower panel shows the results for the cold r process. Dashed lines denote the results obtained with the FRDM decay data, and full lines denote results obtained in the present study.

regions with the longest lifetimes that correspond to the magic shell closures. One can clearly see a correlation between the abundances in Fig. 16 and the average isotopic lifetimes in Fig. 17. While the freeze-out abundance patterns in Fig. 16 are almost identical, the magnitude of the different peaks reflect the local values of the average isotopic lifetimes. Furthermore, the FRDM+QRPA lifetimes are substantially longer for the particularly close to the magic neutron numbers $N = 82$, corresponding to $Z \sim 50$, and $N = 126$, corresponding to $Z \sim 70$.

After freeze-out, the final abundance pattern is shaped during the decay to stability by a global competition between neutron captures and β decays. The earlier freeze-out for D3C* has important consequences for the shaping of the final abundance pattern during the decay to stability. It occurs at a higher value of the density, producing a faster and larger drop in the neutron-to-seed ratio. As a consequence, there is less time for neutron-captures during the freeze-out to move the peaks to higher A values, as discussed in Ref. [3]. These results agree very well with the recent exploration of the effects of β-decay half-lives of very heavy nuclei on the heavy element nucleosynthesis operating in neutron star merger conditions [70]. There, the authors have found the same shift of the third peak towards lighter masses when the faster half-lives are included in the simulation.

The above discussion illustrates the important role of the competition of neutron captures and β decay during freeze-out in shaping the final r-process abundance pattern. It suggest that any sensitivity study of r-process nucleosynthesis should address simultaneously the role of β decays and neutron captures. This aspect will be explored in more detail in a future publication with emphasis in neutron star merger conditions that is currently considered the preferred r-process astrophysical site. An important aspect for r-process calculations under neutron star merger conditions is the nuclear energy generation. It depends mainly on the β-decay rates, and determines the evolution of temperature during the r process [75]. The nuclear energy production is also important to determine the evolution of material ejected in highly eccentric loosely bound orbits. Depending on the energy produced by the r process, this material can become unbound affecting the late-time evolution of short gamma-ray burst afterglows, assuming they are powered by matter fallback [76]. At later times the radioactive heating from the β decay of r-process material will also affect the neutron-star merger remnant

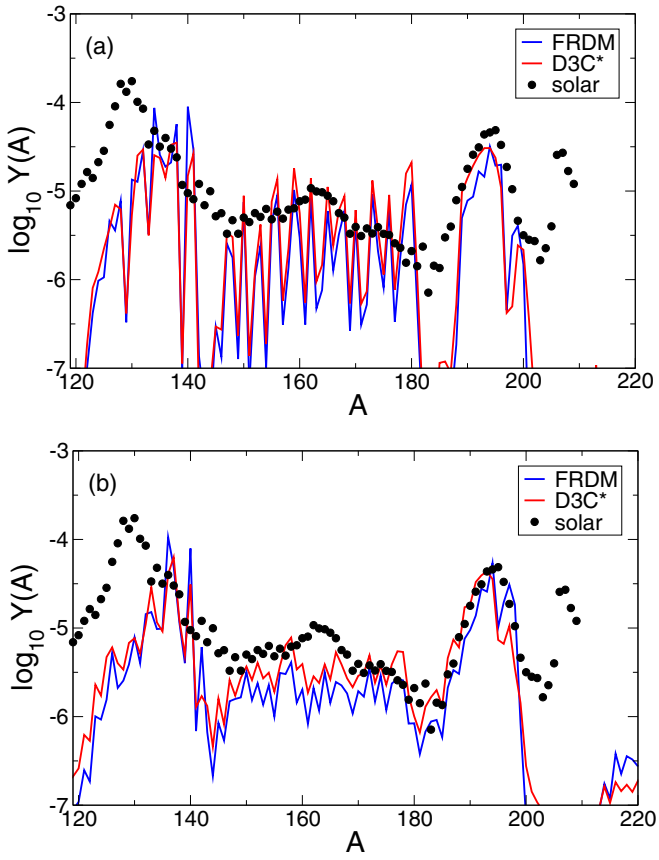

FIG. 16. The abundances of heavy nuclei resulting from a hot r-process (upper panel) or a cold r-process (lower panel) calculation using the half-lives obtained from the FRDM and the current model. The abundances are plotted at the time of the freeze-out, i.e., at the point when the ratio of neutrons to seed nuclei reaches 1. The solid circles denote the solar r-process abundances.

evolution [77] and the electromagnetic transient, or kilonova, light curve [78–80]. For all these applications it is important to know how much of the energy produced by β decay is lost in the form of neutrinos and how the remaining energy is distributed between the electrons and gamma rays emitted from nuclear deexcitation. We have determined for each decay these quantities based on the computed β-decay strengths. A small part of the energy will be carried away by the neutrons emitted after the β decay. Our gamma channel does in fact also include this energy, as it is assumed that the emitted neutrons will thermalize in a relatively short timescale. All this information is included in the Supplemental Material [33], which also includes the relevant β-decay rates.

Figure 18 shows the average energy of electrons, neutrinos, and photons produced after β decay as a function of the decay Q value. The red lines denote the one-half and one-third ratios between the energy and the Q values:

$$\bar{E}^1_{e,\bar{\nu},\gamma}(Q) = \tfrac{1}{2}Q, \quad \bar{E}^2_{e,\bar{\nu},\gamma}(Q) = \tfrac{1}{3}Q. \tag{24}$$

One can see that the ratio of the average electron energy and the nuclear Q value is concentrated around 1/3, while the same ratio for the antineutrinos is in the range 0.3–0.5. r-process

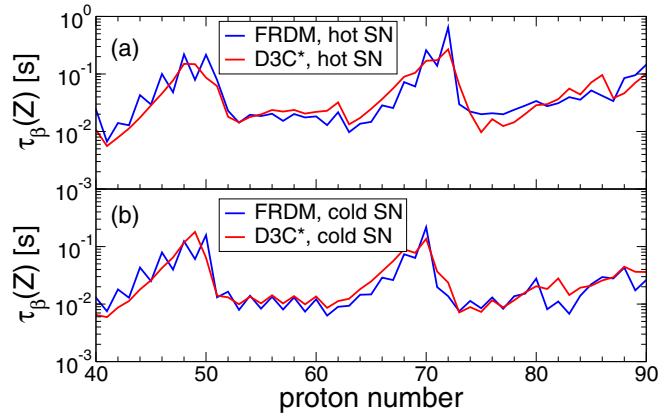

FIG. 17. The isotopic lifetimes defined in Eq. (23) as a function of the atomic number, at the moment of r-process freeze-out. In the top panel we show the results for the hot r process and in the bottom panel the results for the cold r process.

nucleosynthesis is not expected to be sensitive to this range of variations in the heating rate [75]. However, kilonova light curves are more sensitive to this range of variation [78] and our calculations are the first to provide this information for future modeling.

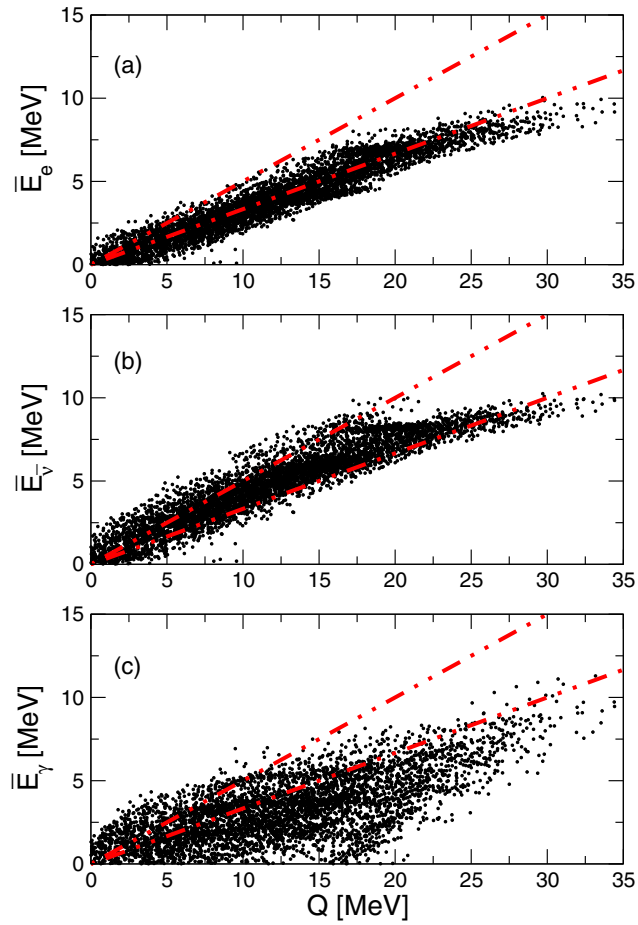

FIG. 18. Average energy of the electrons, neutrinos, and photons produced after β decay.

IV. CONCLUSION AND OUTLOOK

In this study we have performed a large-scale calculation of β-decay rates and β-delayed neutron emission probabilities for neutron-rich nuclei with $8 \leqslant Z \leqslant 110$. A fully self-consistent theoretical framework was employed based on the relativistic nuclear energy density functional. The advantages of this approach are (i) self-consistent modeling of all relevant transition matrix elements without any adjustment of the model parameters to the nucleus under consideration, and (ii) equal treatment of allowed and first-forbidden transitions. The r process involves even-even nuclei, but also odd-A and odd-odd nuclei. It is, therefore, very important that all types of nuclei are treated within a single theoretical framework. We have tested the quality of the description of odd nuclei by comparing the β-decay Q values with those of the FRDM and the data for the silver and cadmium isotopic chains, where the results show very good agreement with the available data. Additionally, in agreement with data there is no noticeable odd-even staggering in the obtained half-lives, and the statistical analysis shows only a small tendency to overestimate the half-lives of odd-Z and odd-odd nuclei. Additionally, even though the model used assumes a spherical shape of the nucleus under consideration, it has been shown that it can accurately describe the reaction rates both in the regions of the nuclear chart close to closed shells and in open-shell nuclei known to be well deformed. Thus, the model employed is shown to reproduce β-decay data across the whole neutron-rich side of the nuclear chart with good precision, regardless of the type of nucleus.

In general, the key features of the decay rates across the nuclear chart have been reproduced. We obtain a very good agreement with the data for isotopic chains with both an even and odd atomic number, without any noticeable odd-even staggering along the chain and closely following the trend of the measurements. This characteristic ensures a smoother behavior during the final decay towards the line of stability in the late stages of the heavy element nucleosynthesis. The FRDM results, however, often display erratic jumps in the half-lives without an underlying physical reason, as is evident in, e.g., strontium and cadmium isotopic chains. In comparison to recent data, both models produce similar discrepancies. In the light nuclei region, both models reproduce the data within a factor of 2, for a wide selection of nuclei with atomic numbers ranging from $Z = 36$ to $Z = 43$. In the region of very heavy nuclei, the FRDM overestimates the half-lives of nuclei below the $Z = 82$ closed proton shell, while the present work provides a reasonable description of the decay properties. However, around the $N = 82$ shell, the D3C* model significantly underestimates the half-lives. Extending the analysis to the whole neutron-rich part of the nuclear chart, we obtain very good agreement with the data, except in the regions just above a closed proton shell but below the next closed neutron shell, i.e., the same regions where the model predicts high contribution of the first-forbidden transitions. We also performed a statistical analysis, where we studied the quality of the half-life predictions with respect to the measurements, depending on the type of nuclei. We obtained a very good average reproduction of the data, with a tendency to overestimate the half-lives of odd-Z nuclei. In contrast with this result, the very good overall agreement of the FRDM predictions with the measurements is a consequence of a cancellation of a significant overestimate of the half-lives of even-Z (especially even-even) nuclei with a smaller underestimate of the half-lives of odd-Z nuclei. In both cases, the description improves for shorter-lived nuclei, due to the importance of the lepton phase space that increases sharply with larger Q values.

The consistent inclusion of the first-forbidden transitions in this study has allowed for a systematic study of the contribution of parity changing transitions to the decay rate for a large number of nuclei. In specific cases, namely the $N = 50$, $N = 82$, and $N = 126$ isotonic chains, the results of the present study agree well with data and results based on other models, except in particular cases such as the nuclei above the $Z = 28$ proton shell where we predict a strong contribution of the forbidden transitions. For $N = 126$ isotones, the model predicts an increase of the contribution of first-forbidden transitions to the total decay rate, in agreement with the results obtained by other models. For nuclei with $N < 126$, we predict a smooth increase of the contribution of the parity changing transitions from the valley of stability towards the neutron drip line, and a saturation at approximately 40%–60% of the total rate. Nuclei with $N > 126$ show a suppression of Gamow-Teller transitions that only became possible by isospin-breaking terms mainly due to Coulomb interaction.

Closely related to β-decay is the process of β-delayed neutron emission, which also affects the late stages of the r process by contributing to the neutron flux and the redistribution of mass. The characteristic quantity is the average number of emitted neutrons, which is a measure of the decay rate that falls above the neutron separation energy. This quantity depends on both the Q value and the one, two, and more neutron separation energies, and displays odd-even staggering both between the isotopic chains and along a particular chain. We have extracted the probabilities for emission of one or more neutrons and the average number of emitted neutrons from the previously calculated decay data. The results show a physical saturation of the average number of emitted neutrons closer to the neutron drip line, which indicates that the decaying matter could provide a significant number of neutrons. In contrast, the FRDM predicts a similar but overall lower number of emitted neutrons per decay, with oscillating behavior close to the neutron drip line.

The present results have been applied in an r-process calculation in hot and cold r-process scenarios corresponding to matter ejected under moderately high entropy. We find substantial changes in the r-process abundances that are mainly due to the fact that for r-process nuclei the present half-lives are systematically shorter than those computed by the FRDM+QRPA approach.

This study has shown that the theoretical framework based on the relativistic nuclear energy density functional is a mature one, capable of providing a good description of sensitive physical quantities. However, the description of half-lives of a large range of nuclei remains challenging, especially for nuclei close to the valley of stability. Further advances in this field will require effort along three possible directions: (i) improving the

relativistic energy density functional will serve to provide more accurate Q_β values and enhance the description of the energy generation during the decay released in the form of electron, antineutrinos and gamma-rays; (ii) a consistent treatment of deformations will be necessary to enhance the description of the transitions in particular open-shell nuclei; and (iii) inclusion of complex-configurations in the QRPA basis will enrich the transition spectrum, especially in the low-energy region, and provide a better description of β decays, but also give information on the detailed structure of the transition strength.

ACKNOWLEDGMENTS

This work was supported in part by the Helmholtz International Center for FAIR within the framework of the LOEWE program launched by the State of Hesse, by the BMBF-Verbundforschungsprojekt No. 06DA7047I, the Helmholtz Association through the Nuclear Astrophysics Virtual Institute (VH-VI-417), by the Croatian Science Foundation under the project IP-2014-09-9159, by IAEA Research Contract No. 18094/R0, and by the DAAD-MZOS bilateral collaboration program.

[1] K. Langanke and G. Martinez-Pinedo, Rev. Mod. Phys. **75**, 819 (2003).
[2] M. Arnould, S. Goriely, and K. Takahashi, Phys. Rep. **450**, 97 (2007).
[3] A. Arcones and G. Martínez-Pinedo, Phys. Rev. C **83**, 045809 (2011).
[4] P. T. Hosmer *et al.*, Phys. Rev. Lett. **94**, 112501 (2005).
[5] P. Hosmer *et al.*, Phys. Rev. C **82**, 025806 (2010).
[6] M. Quinn *et al.*, Phys. Rev. C **85**, 035807 (2012).
[7] M. Madurga *et al.*, Phys. Rev. Lett. **109**, 112501 (2012).
[8] F. Montes *et al.*, Phys. Rev. C **73**, 035801 (2006).
[9] S. Nishimura *et al.*, Phys. Rev. Lett. **106**, 052502 (2011).
[10] I. Dillmann *et al.*, Phys. Rev. Lett. **91**, 162503 (2003).
[11] B. Pfeiffer, K. L. Kratz, F. K. Thielemann, and W. B. Walters, Nucl. Phys. A **693**, 282 (2001).
[12] J. Benlliure *et al.*, J. Phys. Conf. Ser. **337**, 012070 (2012).
[13] G. Benzoni *et al.*, Phys. Lett. B **715**, 293 (2012).
[14] R. Caballero-Folsch *et al.*, arXiv:1511.01296 [nucl-ex].
[15] T. Kurtukian-Nieto *et al.*, Eur. Phys. J. A **50**, 135 (2014).
[16] A. I. Morales *et al.*, Phys. Rev. Lett. **113**, 022702 (2014).
[17] E. Caurier *et al.*, Rev. Mod. Phys. **77**, 427 (2005).
[18] Q. Zhi, E. Caurier, J. J. Cuenca-García, K. Langanke, G. Martínez-Pinedo, and K. Sieja, Phys. Rev. C **87**, 025803 (2013).
[19] P. Möller, B. Pfeiffer, and K.-L. Kratz, Phys. Rev. C **67**, 055802 (2003).
[20] I. N. Borzov, Nucl. Phys. A **777**, 645 (2006).
[21] D.-L. Fang, B. A. Brown, and T. Suzuki, Phys. Rev. C **88**, 034304 (2013).
[22] J. Engel, M. Bender, J. Dobaczewski, W. Nazarewicz, and R. Surman, Phys. Rev. C **60**, 014302 (1999).
[23] T. Nikšić, T. Marketin, D. Vretenar, N. Paar, and P. Ring, Phys. Rev. C **71**, 014308 (2005).
[24] T. Marketin, D. Vretenar, and P. Ring, Phys. Rev. C **75**, 024304 (2007).
[25] Z. Niu *et al.*, Phys. Lett. B **723**, 172 (2013).
[26] N. Paar, D. Vretenar, E. Khan, and G. Colo, Rep. Prog. Phys. **70**, 691 (2007).
[27] I. N. Borzov, Phys. Rev. C **67**, 025802 (2003).
[28] D. Vretenar, A. Afanasjev, G. Lalazissis, and P. Ring, Phys. Rep. **409**, 101 (2005).
[29] N. Paar, T. Nikšić, D. Vretenar, and P. Ring, Phys. Rev. C **69**, 054303 (2004).
[30] T. Marketin, G. Martínez-Pinedo, N. Paar, and D. Vretenar, Phys. Rev. C **85**, 054313 (2012).
[31] N. Paar, D. Vretenar, T. Marketin, and P. Ring, Phys. Rev. C **77**, 024608 (2008).
[32] Y. F. Niu, N. Paar, D. Vretenar, and J. Meng, Phys. Rev. C **83**, 045807 (2011).
[33] See Supplemental Material at http://link.aps.org/supplemental/10.1103/PhysRevC.93.025805 for the complete data set containing β-decay rates, β-delayed neutron-emission probabilities, and released energy for all isotopes considered in this study.
[34] J. Berger, M. Girod, and D. Gogny, Nucl. Phys. A **428**, 23 (1984).
[35] N. Paar, P. Ring, T. Nikšić, and D. Vretenar, Phys. Rev. C **67**, 034312 (2003).
[36] P. Ring and P. Schuck, *The Nuclear Many-Body Problem* (Springer, Berlin, 1980).
[37] G. Audi *et al.*, Chin. Phys. C **36**, 1157 (2012).
[38] P. Möller, J. R. Nix, W. D. Myers, and W. J. Swiatecki, At. Data Nucl. Data Tables **59**, 185 (1995).
[39] S. Goriely, N. Chamel, and J. M. Pearson, Phys. Rev. C **82**, 035804 (2010).
[40] T. Duguet, P. Bonche, P.-H. Heenen, and J. Meyer, Phys. Rev. C **65**, 014310 (2001).
[41] T. Duguet, P. Bonche, P.-H. Heenen, and J. Meyer, Phys. Rev. C **65**, 014311 (2001).
[42] K. Takahashi and K. Yokoi, At. Data Nucl. Data Tables **36**, 375 (1987).
[43] K. Langanke and G. Martínez-Pinedo, At. Data Nucl. Data Tables **79**, 1 (2001).
[44] M. A. Famiano, R. N. Boyd, T. Kajino, K. Otsuki, M. Terasawa, and G. J. Mathews, J. Phys. G Nucl. Part. Phys. **35**, 025203 (2008).
[45] F. Minato and K. Hagino, Phys. Rev. C **80**, 065808 (2009).
[46] H. Behrens and J. Jänecke, *Landoldt-Börnstein Tables, Gruppe I* (Springer, Berlin, 1969), Vol. 4.
[47] J. C. Hardy and I. S. Towner, Phys. Rev. C **79**, 055502 (2009).
[48] A. R. Edmonds, *Angular Momentum in Quantum Mechanics* (Princeton University Press, Princeton, 1960).
[49] J. Beringer *et al.*, Phys. Rev. D **86**, 010001 (2012).
[50] H. Behrens and W. Bühring, Nucl. Phys. A **162**, 111 (1971).
[51] H. Behrens and W. Bühring, *Electron Radial Wave Functions and Nuclear β Decay* (Clarendon, Oxford, 1982).
[52] B. H. Wildenthal, M. S. Curtin, and B. A. Brown, Phys. Rev. C **28**, 1343 (1983).
[53] G. Martínez-Pinedo, A. Poves, E. Caurier, and A. P. Zuker, Phys. Rev. C **53**, R2602 (1996).
[54] N. Paar, T. Suzuki, M. Honma, T. Marketin, and D. Vretenar, Phys. Rev. C **84**, 047305 (2011).
[55] E. K. Warburton, Phys. Rev. C **42**, 2479 (1990).
[56] E. K. Warburton, Phys. Rev. C **44**, 233 (1991).

[57] E. K. Warburton, J. A. Becker, B. A. Brown, and D. J. Millener, Ann. Phys. (N.Y.) **187**, 471 (1988).
[58] E. K. Warburton and I. S. Towner, Phys. Rep. **242**, 103 (1994).
[59] T. Suzuki, T. Yoshida, T. Kajino, and T. Otsuka, Phys. Rev. C **85**, 015802 (2012).
[60] T. Marketin, E. Litvinova, D. Vretenar, and P. Ring, Phys. Lett. B **706**, 477 (2012).
[61] E. Litvinova *et al.*, Phys. Lett. B **730**, 307 (2014).
[62] P. Möller, J. R. Nix, and K.-L. Kratz, At. Data Nucl. Data Tables **66**, 131 (1997).
[63] G. Lorusso *et al.*, Phys. Rev. Lett. **114**, 192501 (2015).
[64] E. Litvinova, Phys. Rev. C **85**, 021303 (2012).
[65] Y. F. Niu, Z. M. Niu, G. Colò, and E. Vigezzi, Phys. Rev. Lett. **114**, 142501 (2015).
[66] M. Liu, N. Wang, Y. Deng, and X. Wu, Phys. Rev. C **84**, 014333 (2011).
[67] C. Bauer *et al.*, Phys. Rev. C **86**, 034310 (2012).
[68] T. R. Rodríguez, Phys. Rev. C **90**, 034306 (2014).
[69] P. Möller and J. Randrup, Nucl. Phys. A **514**, 1 (1990).
[70] M. Eichler *et al.*, Astrophys. J. **808**, 30 (2015).
[71] G. R. Keepin, T. F. Wimett, and R. K. Zeigler, Phys. Rev. **107**, 1044 (1957).
[72] K. Miernik, Phys. Rev. C **88**, 041301 (2013).
[73] K. Miernik, Phys. Rev. C **90**, 054306 (2014).
[74] T. Rauscher and F.-K. Thielemann, At. Data Nucl. Data Tables **75**, 1 (2000).
[75] J. J. Mendoza-Temis, M.-R. Wu, K. Langanke, G. Martínez-Pinedo, A. Bauswein, and H.-T. Janka, Phys. Rev. C **92**, 055805 (2015).
[76] B. D. Metzger, A. Arcones, E. Quataert, and G. Martínez-Pinedo, Mon. Not. R. Astron. Soc. **402**, 2771 (2010).
[77] S. Rosswog *et al.*, Mon. Not. R. Astron. Soc. **439**, 744 (2014).
[78] B. D. Metzger *et al.*, Mon. Not. R. Astron. Soc. **406**, 2650 (2010).
[79] L. F. Roberts, D. Kasen, W. H. Lee, and E. Ramirez-Ruiz, Astrophys. J. **736**, L21 (2011).
[80] A. Bauswein, S. Goriely, and H.-T. Janka, Astrophys. J. **773**, 78 (2013).